IL NUOVO CIMENTO Vol. 35 C, N. 5 Settembre-Ottobre 2012
DOI 10.1393/ncc/i2012-11309-3

Communications: SIF Congress 2011

Strain-induced work function changes in Ge nano-stripes on Si(001) studied by energy-filtered photoelectron emission microscopy

G. M. Vanacore(*)
CNISM, Dipartimento di Fisica, Politecnico di Milano - I-20133 Milan, Italy

ricevuto il 5 Febbraio 2012; approvato il 13 Febbraio 2012

Summary. — Investigation of Ge nanostructures on Si(001) is of great interest for high-mobility Ge MOSFETs and potential applications in near-infrared photodetection. In this paper the experimental investigation of the strain state of Ge nano-stripes fabricated by selective epitaxial growth of Ge on a Si(001) substrate patterned with 100 nm wide trenches is presented. Energy-filtered photoelectron emission microscopy has been used to spatially map with nanoscale resolution the strain-induced change in the electron work function of the nano-stripes. Strain information has been obtained by comparing the experimentally measured work function with a simple model developed within the framework of the potential deformation theory. A tensile deformation of $\sim 0.4\%$ has been found in the nano-stripes. The origin of this strain state is attributed to the joint contribution of the plastic relaxation induced by misfit dislocations and the coherency constraints imposed by the Si substrate, as supported by finite element method (FEM) simulations.

PACS 79.60.Jv – Interfaces; heterostructures; nanostructures.
PACS 73.30.+y – Surface double layers, Schottky barriers, and work functions.
PACS 71.70.Fk – Strain-induced splitting.
PACS 62.23.St – Complex nanostructures, including patterned or assembled structures.

1. – Introduction

The introduction of SiGe heterostructures into main-stream Si technology has been identified as a possible efficient solution to overcome the physical limitations of Si by the possibility of opening new degrees of freedom via band structure engineering. High carrier mobility can be obtained by controlling the strain in the channel of metal oxide semiconductor field-effect transistors (MOSFETs) [1]. Elemental composition and strain

(*) *Present address*: Arthur Amos Noyes Laboratory of Chemical Physics, California Institute of Technology, Pasadena (CA), United States; E-mail: vanacore@caltech.edu

play a major role in tuning the material properties of such devices [2-6]. When the lateral size of the channel is large compared to its thickness, the strain is biaxial and can be fully controlled tuning the composition of the $Si_{1-x}Ge_x$ virtual substrates. For widths of few hundreds of nm and less, the channel strain depends also on the lateral boundary conditions due to elastic and plastic relaxation, resulting in an anisotropic strain condition which can further enhance the carrier mobility due to the warping of the electronic band structure [7-11]. Within this scenario nanoscale Ge structures on Si(001) are of great interest for high-mobility SiGe MOSFETs [12, 13], and for optoelectronics [14], thermoelectrics [15], and near-infrared photodetection applications due to its CMOS process compatibility and its direct bandgap at 0.8 eV [16].

Noninvasive methods for rapid and quantitative surface strain characterization with nanometer scale resolution are lacking. Conventional techniques, mainly X-ray diffraction [17] and Raman spectroscopy [18], do not provide the spatial resolution required for characterization at the submicrometer scale. The lateral resolution has been improved in recent years when the tip of a scanning probe microscope is used to enhance the Raman scattered light [19]. However, in spite of these achievements, the use of such tools for surface strain mapping techniques is very hard to perform due to the long spectrum acquisition times required for each individual surface point.

The lattice deformation has been demonstrated to have a strong influence on the electron work function of the surface structures under investigation [20, 21], and several authors have recently showed that work function measurements can provide the strain characterization of single structures on a nanometer length scale [22, 23]. In recent years, energy-filtered X-ray photoelectron emission microscopy (X-PEEM) has emerged as one of the most promising full-field imaging methods [24-26] being a suitable tool for non-invasive absolute work function measurements with an energy resolution of ~ 20 meV and a spatial resolution of 50–100 nm [27] and with the great advantage to provide also spatially resolved elemental characterization of the investigated structures [28-30].

In this paper, the strain state of Ge nano-stripes fabricated by selective epitaxial growth of Ge on a Si(001) substrate patterned with 100 nm wide trenches is investigated. Strain information has been obtained by comparing the experimentally measured work function of the nano-stripes with a simple model developed within the framework of the potential deformation theory. The derived strain state is then attributed to the joint contribution of plastic relaxation by misfit dislocations and elastic strain modulation induced by the boundary conditions and the lateral confinement, as supported by finite element method (FEM) simulations.

2. – Experiment

Ge nano-stripes have been created by coupling electron-beam lithography (EBL) and Low Energy Plasma Enhanced Chemical Vapour Deposition (LEPECVD) [31]. A Si(001) substrate has been patterned with a series of trenches (depth ~ 100 nm, width ~ 100 nm, period $\sim 1\,\mu$m) aligned along the [110] direction by means of EBL. Then 15 nm of pure Ge have been deposited by LEPECVD with a growth rate of 1.5 nm/s and a substrate temperature of 650 °C. Under these growth conditions the trenches behave as material traps and represent preferential nucleation sites since a total elastic energy minimum is reached at the trench bottom [32]. This favors the gathering of Ge from the surrounding surface area at the trench positions forming embedded nano-stripes. A SiGe epilayer possibly formed in between the structures was completely etched away by a gently mechanical polishing performed after the Ge growth. Figure 1(a) shows the XPEEM image of the

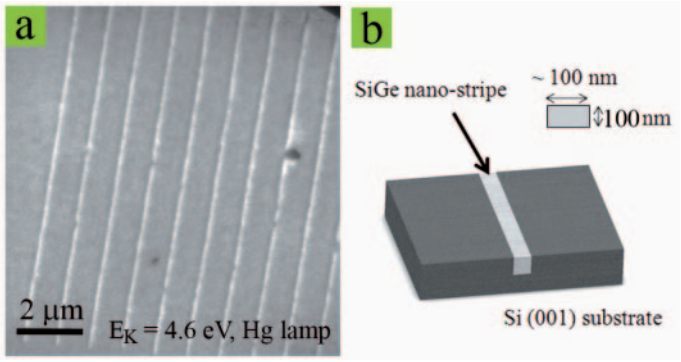

Fig. 1. – Panel (a): XPEEM image of the nano-stripes array with a periodic separation of 1 μm acquired at a kinetic energy of 4.6 eV using Hg as excitation source. Panel (b): schematic representation of the embedded nano-stripes studied in this work.

periodic array of the nano-stripes acquired at a kinetic energy of 4.6 eV (secondary electron detection) using a Hg lamp as excitation source, while in fig. 1(b) the schematic representation of the embedded nano-stripes is shown. It is worth noting that the high growth rate (1.5 nm/s), the moderate substrate temperature (650 °C), and the very short deposition time (10 s) have been used in order to strongly reduce the Si incorporation from the substrate essentially leading to the formation of Ge nano-stripes [33].

The Energy-Filtered XPEEM experiment took place at the TEMPO beamline of SOLEIL Synchrotron using the NanoESCA photoemission microscope (Omicron Nanotechnology). This is composed of a fully electrostatic PEEM column together with an aberration corrected energy filter consisting of two hemispherical electron energy analyzers coupled by a transfer lens. The energy-filtered imaging mode works at high energy and spatial resolution [30]. Soft X-rays with photon energy of 90 eV have been used for the core-level and the work function mapping. The sample was mounted such that the normal to the (001) surface was in the horizontal scattering plane containing the incoming wave vector. The light was hitting the surface at a grazing incidence angle of 23° with respect to the (001) plane, and a horizontal linear polarization of the incident light was chosen in order to have a preferential sensitivity along the out-of-plane direction ([001] direction). The NanoESCA spectro-microscope was operated with a contrast aperture of 70 μm, an extractor voltage of 15 kV, a pass energy of 50 eV, and an entrance analyzer aperture of 1 mm. All images were corrected for the inherent non-isochromaticity [34]. Dark and flat field corrections for camera noise and detector inhomogeneities were also applied.

The preparation protocol for the cleaning of the sample surface used during the XPEEM experiment has been the following: i) chemical etching of the native silicon and germanium oxide by diluted HF (10% for 30 s at RT); ii) UV-ozone treatment by irradiation with D_2 lamp under O_2 flux (15–20 min) for carbon removal [35, 36]; iii) removal of silicon oxide layer (covering the surface after the UV treatment) by *in situ* mild Ar^+ sputtering (beam voltage $\sim$ 500–1000 V, beam current $\sim$ 1 μA), and iv) thermal relaxation by *in situ* annealing below the diffusion threshold temperature ($\sim$ 400 °C).

3. – Results

The XPEEM results are image series across the spectrum of interest in the form of three-dimensional (3D) data sets of the photoemission intensity $I(p_x, p_y, E_K)$ as

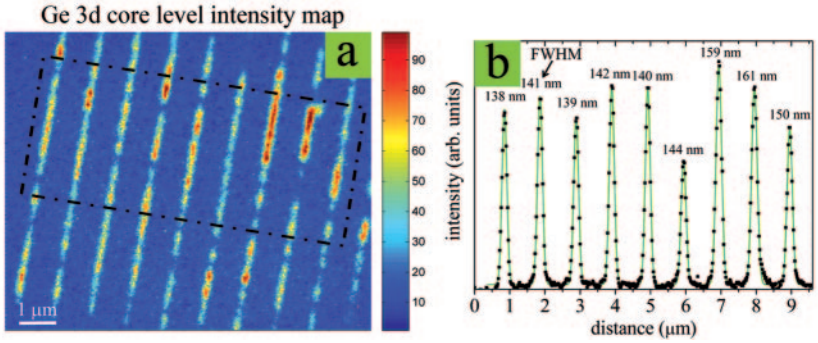

Fig. 2. – (Colour on-line) Panel (a): Ge 3d core level map obtained by acquiring photoelectrons energy filtered images and monitoring the intensity of the pixel-by-pixel Ge 3d spectra extracted over the FoV. Panel (b): cross-section profile of Ge 3d intensity plotted along the direction perpendicular to the stripes (black squares), together with the best fitting of the experimental data using a Gaussian function for each stripe (green solid line). The full width half maximum (FWHM) obtained for each stripe is also reported. The de-convolution of the experimentally measured profile across the 100 nm wide stripes allowed to estimate the spatial resolution achieved in the X-PEEM experiment to be less than 100 nm.

a function of the kinetic energy, E_K, and of the position, p_x and p_y, within the field of view (FoV).

The elemental distribution mapping of the nano-stripes has been obtained by acquiring photoelectrons energy filtered images around the Ge 3d core level (binding energy, $E_B \sim 29\,\text{eV}$). Figure 2(a) represents the Ge 3d core level map, obtained by monitoring the intensity of the pixel-by-pixel Ge 3d spectra extracted over the FoV. This shows an almost homogeneous filling of the lithographically made trenches without any Ge overflowing in the region between them, confirming their behavior as material traps. In fig. 2(b) is reported the cross-section profile of Ge 3d intensity along the direction perpendicular to the stripes (black squares), together with the best fitting of the experimental data using a Gaussian function for each stripe (green solid line). The deconvolution of the experimentally measured profile across the 100 nm wide stripes allowed to estimate the spatial resolution achieved in the X-PEEM experiment to be less than 100 nm.

With a photon energy of 90 eV, the photoemission threshold represents a true secondary electron (SE) peak and direct transitions play no part in the intensity position. Thus the position of the threshold in the local spectra extracted from photoelectron image series across the SE peak is equivalent to the work function (after correction for the Schottky effect due to the high surface potential created by the extractor [37]: $\Delta E_{\text{Schottky}} = 0.11\,\text{eV}$ for 15 kV). In general, the work function, Φ, is defined as the energy needed to promote an electron from the Fermi level to the vacuum level: $\Phi = E_0 - E_F$, where E_0 is the vacuum level and E_F is the Fermi level of the sample surface. Figure 3(a) shows the secondary electron distribution spectra extracted from the Si bulk and from a single nano-stripe, where the energy scale on the abscissa axis is represented by the final state energy, E, referred to the Fermi level, E_F. These distributions are very similar to those reported by several authors [30, 38, 39]. The local work function map (see fig. 3(b)) of the Si substrate and of the Ge nano-stripes has been obtained from the best least-square fitting of the experimental pixel-by-pixel spectra to the secondary electron

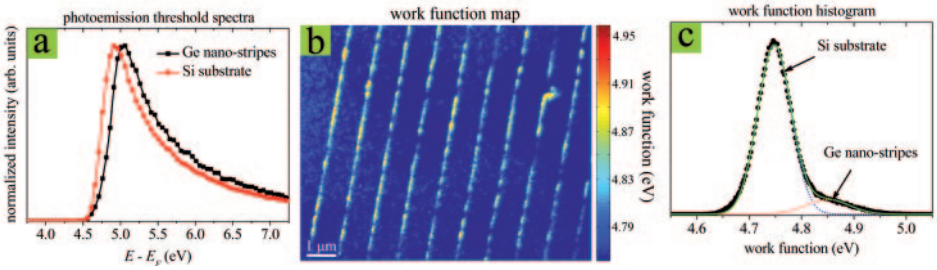

Fig. 3. – (Colour on-line) Panel (a): experimental secondary electron energy distributions as a function of $E - E_F$ for the Si bulk (red circles) and for a single Ge nano-stripe (black squares). Panel (b): work function map after correction for the Schottky effect obtained from the least-square fitting of the pixel-by-pixel experimental threshold spectra to the secondary electron distribution described by Henke's model (see text). Panel (c): work function histogram derived from the spatial mapping presented in the panel (b). The histogram is composed by two Gaussian distributions centered at ~ 4.74 eV and ~ 4.85 eV associated to the Si bulk and to the Ge nano-stripes, respectively.

distribution, $S(E - E_F)$, described by Henke *et al.* [40]:

$$S(E - E_F) = \frac{A(E - E_F - \Phi)}{(E - E_F - \Phi + B)^4}\,, \tag{1}$$

where A is a scaling factor and B is a fitting parameter. From the work function map in fig. 3(b) and the relative histogram in fig. 3(c), where two separated features related to the substrate and to the nano-stripes are clearly visible, we obtain $\Phi_{\text{substrate}} = 4.74 \pm 0.02$ eV for the Si substrate and $\Phi_{\text{stripe}} = 4.85 \pm 0.02$ eV for the nano-stripes. The work function value for the substrate is consistent with that reported in case of pure bulk intrinsic Si(001) (4.75 eV) [41], while the work function value measured for the Ge stripes is larger by about 80 meV than that one of the bulk Ge(001) (4.77 eV) [42]. Several factors may affect the work function and recent experiments based on Kelvin Probe Force Microscopy (KPFM) [22,23] and *ab initio* calculations [21] showed that it exhibits significant changes as a function of the strain of the investigated structures. Work function changes due to oxidation of Ge(001) surface has been also extensively reported [43]. In our case we can exclude the presence of germanium-oxide contamination on the Ge nano-stripes since no chemical shifted structures appears at the low kinetic energy side in the Ge 3d spectrum.

4. – Discussion

The strain-induced work function modification would reflect: i) the variation of the surface electrostatic dipole due to the charge redistribution in the last monolayer as the lattice is deformed [20,21], and ii) the shift of the Fermi Level with respect to the vacuum level due to the warping of the band structure [44, 45]. In the following discussion the measured work function change for the Ge nano-stripes with respect to the bulk case is related to the strain in the nano-stripes by developing a simple model able to take into account both effects.

The dipole contribution to the work function change is often calculated on the basis of simplified assumptions about the nature and the magnitude of the dipoles. In a simple

model one can describe the dipole effect in terms of emitted electrons crossing a parallel-plate capacitor (plate separation d), which carries a total surface charge density σ_{dip}. At first-order approximation, σ_{dip} can be considered to change linearly with the hydrostatic lattice distortion ε_h [46]:

$$\sigma_{\mathrm{dip}} = \sigma_0[1 - k_s\varepsilon_h],$$

where σ_0 is the surface charge density for the unstrained crystal lattice, $\varepsilon_h = (\varepsilon_{xx} + \varepsilon_{yy} + \varepsilon_{zz})/3$, and $k_s = -\frac{\Delta\sigma/\sigma_0}{\varepsilon_h}$ (with $\Delta\sigma = \sigma_{\mathrm{dip}} - \sigma_0$) is the variation rate. Thus the strain-induced variation of the surface dipole contribution to the work function is given by

$$\Delta\Phi_{\mathrm{dip}} = e\frac{\Delta\sigma}{\varepsilon_r\varepsilon_0}d = -e\frac{\sigma_0 k_s\varepsilon_h}{\varepsilon_r\varepsilon_0}d,$$

where e is the electron charge, ε_0 is the vacuum permittivity, ε_r is the Ge dielectric constant, and the dipole separation $d \approx a_{\mathrm{Ge}}/4$ (where $a_{\mathrm{Ge}} = 5.658\,\text{Å}$ is the lattice parameter of unstrained Ge) is considered to be independent of the lattice distortion. The surface charge density for the unstrained lattice, σ_0, is derived by the recent experimental study of Ciston *et al.* [47], who coupled X-ray diffraction data with *ab initio* calculations. The variation rate k_s is obtained assuming that the surface charge density and the volume charge density change with the lattice distortion in the same way, *i.e.* $k_s = -\frac{\Delta\sigma/\sigma_0}{\varepsilon_h} \approx -\frac{\Delta\rho/\rho_0}{\varepsilon_h} = k_v$, where ρ is the volume charge density. The parameter k_v can be derived from the first-principles calculations of Aourag *et al.* [48], who calculated the electronic structure of Si as a function of its lattice parameter. Thus, a direct quantification of the strain-induced variation of the surface dipole contribution to the work function is obtained: $\Delta\Phi_{\mathrm{dip}} = -(4.036\,\mathrm{eV} \pm 0.343\,\mathrm{eV})\varepsilon_h$, where the uncertainty is based on the error for the evaluation of σ_0 and k_s parameters. This result is consistent with the following picture: under tensile distortion ($\varepsilon_h > 0$) less electronic charge density is distributed outside the surface reducing the dipole strength and thus lowering the work function, while a compressive strain ($\varepsilon_h < 0$) would cause an opposite behavior and thus an increase of the work function.

Besides the surface effects, a further contribution to the work function change is the shift in the Fermi level due to strain-induced warping of the band structure. A crystal lattice distortion is responsible for a strong modification of the electronic band structure: the hydrostatic component affects the bands offset, while the uniaxial component is responsible for the splitting of degenerate bands. Strain and modification of the crystal's band structure are related through the linear deformation theory [49]. Within this framework the conduction and valence band shifts due to the combined contribution of uniaxial strain and hydrostatic strain are [49]

$$\Delta E_{CB} = a_C 3\varepsilon_h + \Delta E_{CB}^{uni},$$
$$\Delta E_{VB} = a_V 3\varepsilon_h + \Delta E_{VB}^{uni}$$

where a_C and a_V are the dilatation deformation potentials for the conduction and valence bands, respectively ($a_C = -8.24\,\mathrm{eV}$, $a_V = 1.24\,\mathrm{eV}$) [49], while $\Delta E_{CB}^{\mathrm{uni}}$ and $\Delta E_{VB}^{\mathrm{uni}}$ represent the shift contributions due to the uniaxial strain component along the stripe axis ($[1\bar{1}0]$ direction) and are calculated using the procedure detailed in ref. [49]. Assuming that the nano-stripes are intrinsic, the strain-induced Fermi level shift, ΔE_F, is thus

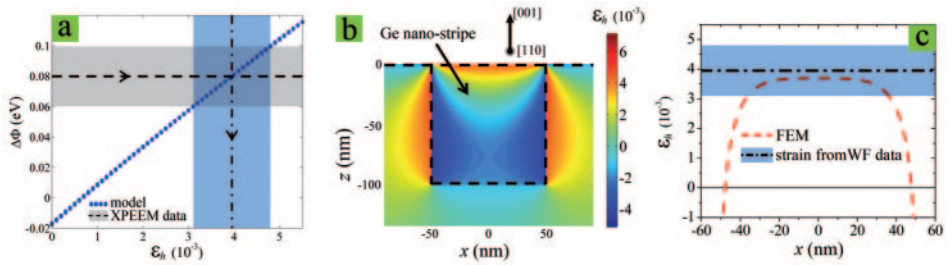

Fig. 4. – (Colour on-line) Panel (a): blue circles represent the work function change as a function of the hydrostatic strain component, ε_h, as obtained by the model developed in the text. The comparison between the calculated and the experimentally measured work function change (shown as black horizontal dashed line and grey shaded region) allows the determination of the strain state of the Ge nano-stripes. Panel (b): spatial map of the hydrostatic deformation, ε_h, in the xz plane obtained by FEM simulation under coherent boundary conditions in the hypothesis that $\varepsilon_{xx} \approx \varepsilon_{yy} \approx 0$ at the stripe/substrate interface in order to take into account the plastic relaxation by misfit dislocations. Panel (c): the red dashed line represents the calculated ε_h strain profile of the Ge nano-stripes. This has been derived by FEM simulations presented in the panel (b) averaging the ε_h map along the out-of-plane direction and weighting the strain values at different depth with an exponential curve with an attenuation length of ~ 6 nm. The strain value obtained by comparing the experimental work function change with the analytical model is also shown as horizontal black dash-dotted line and blue shaded region.

given by

$$\Delta E_F = \frac{1}{2}\left(\Delta E_{CB} + \Delta E_{VB}\right).$$

A negative shift means that the Fermi level is moving downward with respect to the vacuum level, and thus the work function would become greater by the same amount, so that: $\Delta\Phi_{\text{Fermi}} = -\Delta E_F$.

The blue circles in fig. 4(a) show the work function change, $\Delta\Phi = \Delta\Phi_{\text{dip}} + \Delta\Phi_{\text{Fermi}}$, as a function of the hydrostatic strain component, ε_h, due to the joint contribution of the surface dipole variation and the Fermi level shift. The comparison between the calculated and the experimentally measured work function changes allows the determination of the strain state of the Ge nano-stripes: the strain is tensile with a hydrostatic component $\varepsilon_h \approx 3.95 \pm 0.85 \times 10^{-3}$.

In the following the origin of this tensile deformation is discussed. The coherency constraint imposed by the Si substrate generates a compressively strained state of the epitaxially grown stripes. The free surface allows for a partial elastic relaxation generating a tetragonal deformation in an attempt to conserve the unit-cell volume. Redistribution of the elastic energy between the stripe and the substrate also occurs, inducing a strong spatial modulation of the elastic field along both in-plane and out-of-plane directions, as can be seen in fig. 4(b) showing the calculated spatial map of the ε_h strain component in a plane perpendicular to the stripe axis ($[1\bar{1}0]$ direction) under coherent boundary conditions. The calculated strain map was obtained by using linear elasticity theory solved by Finite Element Methods (FEM), exploiting the OpenFOAM package [50], and by using isotropic elastic constants. Together with elastic relaxation, an additional strain relief channel can be opened by the formation of misfit dislocations (plastic relaxation) as driven by the tendency towards the lowering of the elastic budged. The thickness of the Ge stripes studied in this work is definitely larger than the critical thickness for

dislocation injection in Ge [51]. Thus, misfit dislocations are likely to nucleate inside the stripes, running parallel and perpendicular to their axis, although their final density is strongly dependent on the shape and size of the trenches [51]. To include in a first-order approximation the effect of the plastic relaxation into the FEM simulations, we assumed as a fixed constraint that at the stripe/substrate interface the strain along the stripe axis, ε_{yy}, and along the stripe width direction, ε_{xx}, is fully relaxed ($\varepsilon_{yy} = \varepsilon_{xx} = 0$). The red dashed line in fig. 4(c) represents the FEM calculated hydrostatic strain profile under this condition. This behavior has been obtained by averaging the calculated ε_h within the stripe along the out-of-plane direction, and weighting the strain values at different depth with an exponential curve inside the Ge stripe with an attenuation length of ~ 6 nm (this value corresponds to the inelastic mean free path of electrons with a kinetic energy of ~ 4.85 eV propagating in Ge along the direction normal to the surface) [52]. The simulated FEM results reasonably agree with the strain value obtained by the work function data, represented by the black dash-dotted line and the blue shaded area in fig. 4(c). The final strain state should be thus understood as a superposition of two contributions: i) a nearly fully plastic relaxation by misfit dislocations, and ii) an elastic strain modulation induced by the vertical lateral walls which is able to induce a larger lattice deformation with respect to the cases of a two-dimensional thin films [44] ($\varepsilon_h \sim 1 \times 10^{-3}$) and of Ge-rich SiGe islands [33] ($\varepsilon_h \sim 1.7 \times 10^{-3}$).

5. – Conclusions

In this paper the spatial mapping with nanoscale resolution of the elemental distribution and of the electron work function of lithographically defined 100 nm wide Ge nano-stripes has been presented using energy-filtered X-ray photoelectron emission microscopy. A positive shift for the work function of the nano-stripes of ~ 0.08 eV with respect to the unstrained Ge(001) is measured. By comparing the experimentally measured work function change with a simple model developed within the framework of the potential deformation theory, it has been determined that the nano-stripes exhibit a tensile deformation with a hydrostatic strain component of $\sim 3.95 \pm 0.85 \times 10^{-3}$, larger than the case of two-dimensional thin films and Ge-rich SiGe islands. This strain state is consistent with the superposition of two contributions: i) a nearly fully plastic relaxation by misfit dislocations, and ii) an elastic strain modulation induced by the boundary conditions and the lateral confinement. Finite element method simulations are successfully compared to the experimental results.

* * *

Very special thanks are due to N. Barrett, O. Renault, M. Lavayssierre, and F. Sirotti for assistance with the experiments, to M. Bollani, D. Chrastina, and G. Isella for the sample preparation, and to F. Boioli, F. Montalenti, A. Tagliaferri and M. Zani for valuable discussions.

REFERENCES

[1] Irisawa T., Numata T., Tezuka T., Usuda K., Sugiyama N. and Takagi S.-I., *IEEE Trans. Electron Devices*, **55** (2008) 649.

[2] Zhu G. H., Lee H., Lan Y. C., Wang X. W., Joshi G., Wang D. Z., Yang J., Vashaee D., Guilbert H., Pillitteri A., Dresselhaus M. S., Chen G. and Ren Z. F., *Phys. Rev. Lett.*, **102** (2009) 196803.

[3] Broido D. A., Malorny M., Birner G., Mingo N. and Stewart D. A., *Appl. Phys. Lett.*, **91** (2007) 231922.
[4] Landry E. S. and McGaughey A. J. H., *Phys. Rev. B*, **79** (2009) 075316.
[5] Stangl J., Holý V. and Bauer G., *Rev. Mod. Phys.*, **76** (2004) 725.
[6] Bonera E., Pezzoli F., Picco A., Vastola G., Stoffel M., Grilli E., Guzzi M., Rastelli A., Schmidt O. G. and Miglio L., *Phys. Rev. B*, **79** (2009) 075321.
[7] Thompson S. E., Sun G., Choi Y. S. and Nishida T., *IEEE Trans. Electron Devices*, **53** (2006) 1010.
[8] Buca D., Holländer B., Feste S., Lenk St., Trinkaus H., Mantl S., Loo R. and Caymax M., *Appl. Phys. Lett.*, **90** (2007) 032108.
[9] Fischetti M. V. and Laux S. E., *J. Appl. Phys.*, **80** (1996) 2234.
[10] Xiang J., Lu W., Hu Y., Wu Y., Yan H. and Lieber C. M., *Nature*, **441** (2006) 489.
[11] Ko H., Takei K., Kapadia R., Chuang S., Fang H., Leu P. W., Ganapathi K., Plis E., Kim H. S., Chen S.-Y., Madsen M., Ford A. C., Chueh Y.-L., Krishna S., Salahuddin S. and Javey A., *Nature*, **468** (2010) 286.
[12] Khakifirooz A. and Antoniadis D. A., *Tech. Dig. - Int. Electron Devices Meet.* **2006**, 667.
[13] Antoniadis D. A., Aberg I., Ni Chleirigh C., Nayfeh O. M., Khakifirooz A. and Hoyt J. L., *IBM J. Res. Dev.*, **50** (2006) 363.
[14] Nataraj L., Sustersic N., Coppinger M., Gerlein L. F., Kolodzey J. and Cloutier S. G., *Appl. Phys. Lett.*, **96** (2010) 121911.
[15] Mingo N., Hauser D., Kobayashi N. P., Plissonnier M. and Shakouri A., *Nano Lett.*, **9** (2009) 711.
[16] Hartmann J. M., Abbadie A., Papon A. M., Holliger P., Rolland G., Billon T., Fédéli J. M., Rouvière M., Vivien L. and Laval S., *J. Appl. Phys.*, **95** (2004) 5905.
[17] Schulli T. U., Stangl J., Zhong Z., Lechner R. T., Sztucki M., Metzger T. H. and Bauer G., *Phys. Rev. Lett.*, **90** (2003) 066105.
[18] Pezzoli F., Bonera E., Grilli E., Guzzi M., Sanguinetti S., Chrastina D., Isella G., von Kanel H., Wintersberger E., Stangl J. and Bauer G., *J. Appl. Phys.*, **103** (2008) 093521.
[19] Ogawa Y., Toizumi T., Minami F. and Baranov A. V., *Phys. Rev. B*, **83** (2011) 081302(R).
[20] Sekiba D., Yoshimoto Y., Nakatsuji K., Takagi Y., Iimori T., Doi S. and Komori F., *Phys. Rev. B*, **75** (2007) 115404.
[21] Leu P. W., Svizhenko A. and Cho K., *Phys. Rev. B*, **77** (2008) 235305.
[22] Unal K. and Wickramasinghe H. K., *Appl. Phys. Lett.*, **90** (2007) 113111.
[23] Shusterman S., Raizman A., Sher A., Paltiel Y., Schwarzman A., Lepkifker E. and Rosenwaks Y., *Nano Lett.*, **7** (2007) 2089.
[24] Rempfer G. F., Skoczylas W. P. and Hayes Griffith O., *Ultramicroscopy*, **36** (1991) 196.
[25] Swiech W., Fecher G. H., Ziethen C., Schmidt O., Schonhense G., Grzelakowski K. M., Schneider C., Fromter R., Oepen H. P. and Kirschner J., *J. Electron Spectrosc. Relat. Phenom*, **84** (1997) 171.
[26] Bauer E., Koziol C., Lilienkamp G. and Schmidt T., *J. Electron Spectrosc. Relat. Phenom.*, **84** (1997) 201.
[27] Renault O., Brochier R., Roule A., Haumesser P.-H., Krömker B. and Funnemann D., *Surf. Interface Anal.*, **38** (2006) 375.
[28] Ratto F., Locatelli A., Fontana S., Kharrazi S., Ashtaputre S., Kulkarni S. K., Heun S. and Rosei F., *Small*, **2** (2006) 401.
[29] De la Pena F., Barrett N., Zagonel L.-F., Walls M. and Renault O., *Surf. Sci.*, **604** (2010) 1628.
[30] Bailly A., Renault O., Barrett N., Zagonel L. F., Gentile P., Pauc N., Dhalluin F., Baron T., Chabli A., Cezar J. C. and Brookes N. B., *Nano Lett.*, **8** (2008) 3709.
[31] Isella G., Chrastina D., Rössner B., Hackbarth T., Herzog H.-J., König U. and von Känel H., *Solid-State Electron.*, **48** (2004) 1317.

[32] Zhong Z., Schwinger W., Schäffler F., Bauer G., Vastola G., Montalenti F. and Miglio L., *Phys. Rev. Lett.*, **98** (2007) 176102.
[33] Bollani M., Chrastina D., Fedorov A., Sordan R., Picco A. and Bonera E., *Nanotechnology*, **21** (2010) 475302.
[34] Escher M., Winkler K., Renault O. and Barrett N., *J. Electron Spectrosc. Relat. Phenom.*, **178-179** (2010) 303.
[35] Fominski V. Yu., Naoumenko O. I., Nevolin V. N., Alekhin A. P., Markeev A. M. and Vyukov L. A., *Appl. Phys. Lett.*, **68** (1996) 2243.
[36] Choi K., Ghosh S., Lim J. and Lee C. M., *Appl. Surf. Sci.*, **206** (2003) 355.
[37] Guth E. and Mullin C. J., *Phys. Rev.*, **59** (1941) 867.
[38] Henke B. L., Smith J. A. and Attwood D. T., *J. Appl. Phys.*, **48** (1977) 1852.
[39] Barrett N., Rault J., Krug I., Vilquin B., Niu G., Gautier B., Albertini D., Lecoeure P. and Renault O., *Surf. Interface Anal.*, **42** (2010) 1690.
[40] Henke B. L., Liesegang J. and Smith S. D., *Phys. ReV. B: Condens. Matter Mater. Phys.*, **19** (1979) 3004.
[41] Novikov A., *Solid-State Electron.*, **54** (2010) 8.
[42] Dillon J. A. and Farnsworth H. E., *J. Appl. Phys.*, **28** (1957) 174.
[43] Surnev S., *Surf. Sci.*, **282** (1993) 10.
[44] Shan B. and Cho K., *Phys. Rev. Lett.*, **94** (2005) 236602.
[45] Ishikawa Y., Wada K., Liu J., Cannon D. D., Luan H.-C., Michel J. and Kimerling L. C., *J. Appl. Phys.*, **98** (2005) 013501.
[46] Weissmüller J., Viswanath R. N., Kramer D., Zimmer P., Würschum R. and Gleiter H., *Science*, **300** (2003) 312.
[47] Ciston J., Subramanian A., Robinson I. K. and Marks L. D., *Phys. Rev. B*, **74** (2006) 085401.
[48] Aourag H., Khelifa B., Sellal F. and Merad G., *Mat. Chem. Phys.*, **28** (1991) 331.
[49] Van de Walle C., *Phys. Rev. B*, **39** (1939) 1871.
[50] `www.openfoam.com`.
[51] Kim M., Hashemi P. and Hoyt J. L., *App. Phys. Lett.*, **97** (2010) 262106.
[52] Tanuma S., Powell C. J. and Penn D. R., *Surf. Interface Anal.*, **43** (2011) 689.